COMMUNICATION

Cyclotriphosphazene-based organic frameworks as third-order nonlinear optical materials†

Suresh Bommakanti,‡[a] Satyapriya Nath,‡[ac] Rudrashish Panda,[b] Ritwick Das [ID] *[bce] and Bishnu P. Biswal [ID] *[acd]

A cyclotriphosphazene (CTP) core as a new NLOphore has been introduced to construct imine (CTP-TAPB) and vinylene-linked (CTP-TCPB) frameworks. The open aperture (OA) femtosecond (fs) Z-scan measurements resulted in the NLO absorption coefficients (β) of -0.023 and -0.019 cm GW^{-1}, whereas the closed aperture (CA) Z-scan transmission measurements yielded a nonlinear refractive index (n_2) of -2.12×10^{-7} and -1.62×10^{-7} cm^2 GW^{-1} for CTP-TAPB and CTP-TCPB, respectively. This resulted in third-order nonlinear susceptibility ($\chi^{(3)}$) of -9.92×10^{-8} and -7.58×10^{-8} esu for CTP-TAPB and CTP-TPCB. The measured values for β and n_2 (or $\chi^{(3)}$) are attributed to the pure electronic excitations owing to the ultrashort timescales (fs) and it is ensured that the contribution from thermo-optic nonlinearities is negligible.

Organic frameworks, such as covalent organic frameworks (COFs)[1] and porous organic frameworks (POFs)[2] are emerging as promising materials for nonlinear optical (NLO) applications in the field of optoelectronics.[3] The NLO responses primarily stem from NLOphores (chromophores exhibiting NLO responses) and are further intensified in these frameworks.[4] This is due to the rigid structure of the frameworks enabling the incorporation of a substantial number of NLO active centers without the risk of aggregation, a limitation often encountered with small organic molecules. Moreover, the inherent rigidity of

the framework facilitates efficient charge distribution along the π-conjugated backbone, leading to a significant increase in NLO response per chromophore.[5] In the case of ordered frameworks such as MOFs and COFs, the unidirectional alignment of the individual dipole moments within their coherent domain plays a crucial role in enhancing the overall NLO response.[6]

In 2019, we successfully synthesised a series of crystalline and amorphous organic frameworks based on porphyrin and conducted a comprehensive investigation into their third-order NLO response.[7] Our findings revealed significantly higher nonlinear absorption (NLA) coefficient values compared to discrete porphyrin molecules. Notably, these framework materials demonstrated intensity-dependent optical switching, showcasing their potential suitability for use in optical-limiting devices. In another noteworthy work, Wang *et al.* reported the development of an sp^3 carbon-linked organic framework incorporating phthalocyanine, exhibiting a commendable NLO response and low optical limiting threshold.[8] Leveraging the facile tunability of organic monomers, Deng *et al.* explored the impact of conjugation length, electronic motif, and crystalline domain on the NLO response of COFs.[9] While the initial proof-of-concept studies in this field are captivating, it is worth noting that only a limited number of NLOphores have been investigated as building units for synthesising organic frameworks through bottom-up approaches.[9,10] Our recent minireview provides a comprehensive overview of the progress made in developing organic frameworks as NLO materials and highlighting the associated challenges.[11] Given that this research area is in its early stages, it is highly imperative to explore new NLOphores as potential building units and systematic structure–property analysis is crucial for advancing this evolving research field.

In this work, we have explored an inorganic–organic hybrid building unit, hexa(4-formyl-phenoxy)cyclotriphosphazene (CTP-6-CHO), comprising a cyclotriphosphazene (CTP) ring, as an NLOphore for designing organic frameworks. Notably, CTPs containing the N$_3$P$_3$ core have been known to show interesting NLO responses.[12] The partially delocalised CTP ring is composed of alternating nitrogen and phosphorus atoms, acting as donor

[a] *School of Chemical Sciences, National Institute of Science Education and Research Bhubaneswar, Jatni, Khurda, Odisha, 752050, India.*
E-mail: bp.biswal@niser.ac.in

[b] *School of Physical Sciences, National Institute of Science Education and Research Bhubaneswar, Jatni, Khurda, Odisha, 752050, India.*
E-mail: ritwick.das@niser.ac.in

[c] *Homi Bhabha National Institute, Training School Complex, Anushakti Nagar, Mumbai, 400094, India*

[d] *Centre for Interdisciplinary Sciences, National Institute of Science Education and Research Bhubaneswar, Jatni, Khurda, Odisha, 752050, India*

[e] *Optics and Photonics Centre, Indian Institute of Technology Delhi, Hauz Khas, New Delhi 110 016, India*

† Electronic supplementary information (ESI) available. See DOI: https://doi.org/10.1039/d3ma01015e

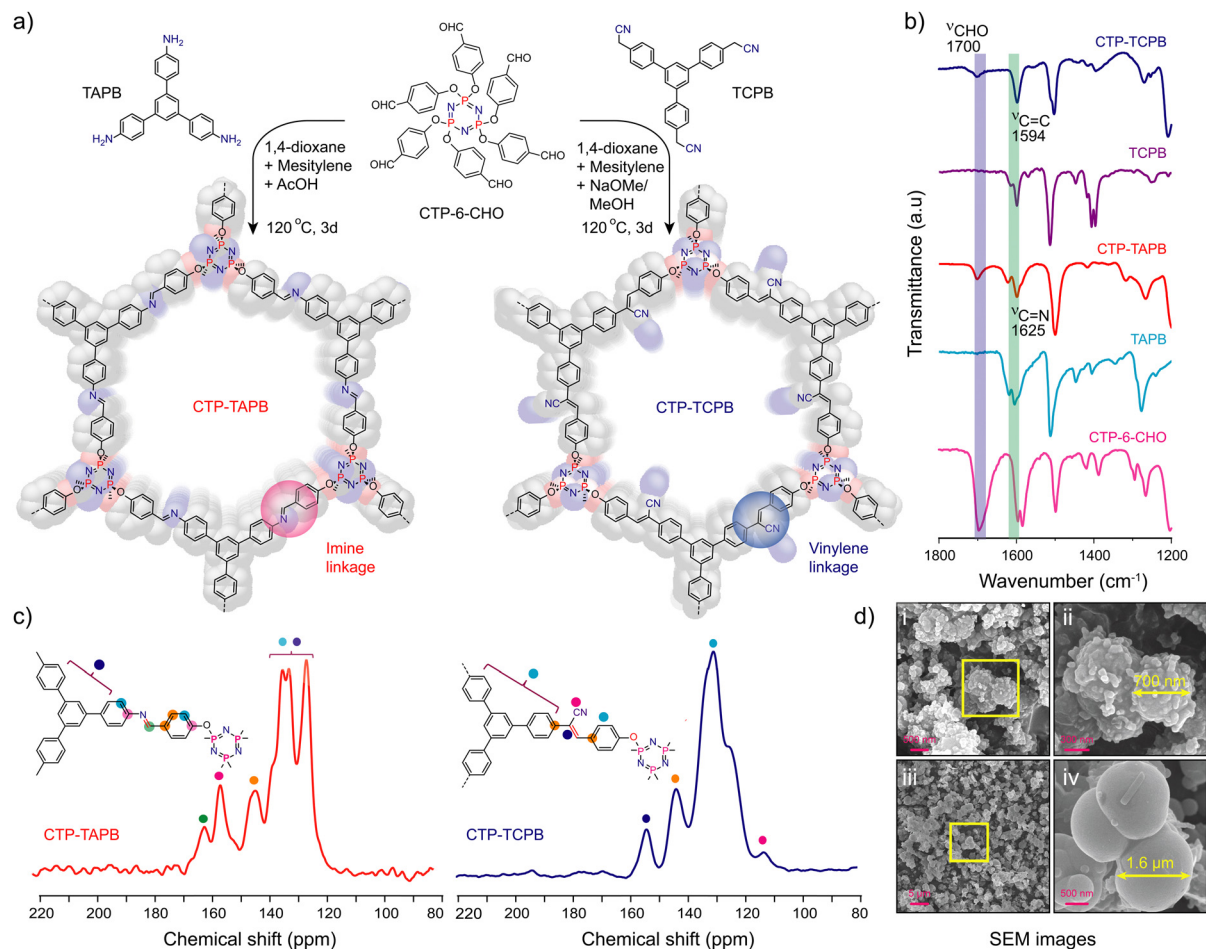‡ S. B. and S. N. contributed equally to this work.

Fig. 1 (a) Schematic representation of the synthesis of organic frameworks; (b) FT-IR spectra including the corresponding monomers; (c) ^{13}C CP-MAS solid-state NMR spectra; and (d) SEM images of CTP-TAPB (i) and (ii) and CTP-TCPB (iii) and (iv) frameworks, respectively.

(D) and acceptor (A) sites, forming a multi-branched octupolar chromophore unit. In this context, CTP-6-CHO was utilised to synthesise two isoreticular organic frameworks: CTP-TAPB and CTP-TCPB with triphenylbenzene (TPB) as the model knot having distinct linkages in their frameworks (Fig. 1a). Furthermore, we have examined the third-order NLO response of the prepared frameworks by deploying an open aperture (OA) Z-scan technique using an ultrashort pulsed fibre laser emitting pulses at 370 fs at 1 kHz repetition rate.

Interestingly, the frameworks (CTP-TAPB and CTP-TCPB) exhibited intensity-dependent optical switching from saturable absorption (SA) to reverse saturable absorption (RSA). Consequently, the NLO absorption coefficient (β) values of 0.023 and 0.019 cm GW^{-1} were deduced, respectively. At ultrashort time scales, the impact of thermo-optic manifestations is negligible, resulting in small negative values for β owing to pure electronic origin. In contrast, nanosecond (ns) laser excitation results exhibited higher values ($\beta \sim 10^4$ cm GW^{-1}) attributed to the dominant contribution from accumulated thermal effects. Thus, these results, SA to RSA switching of CTP-organic frameworks, manifest the potential in optical limiting NLO applications.

Schiff base condensation of CTP-6-CHO and 1,3,5-tris-(4-aminophenyl)benzene (TAPB) in the presence of aqueous acetic acid yielded CTP-TAPB. In contrast, the vinylene-linked CTP-TCPB was obtained through the Knoevenagel condensation of CTP-6-CHO and 1,3,5-tris-(4-cyanomethylphenyl)benzene (TCPB) (Fig. 1a). The detailed synthesis procedures are given in Section S2, ESI.†

To get structural insights into the frameworks, powder X-ray diffraction (PXRD) experiments and structure modelling have been done. The PXRD indicates low crystallinity due to non-planar/ complexity of the CTP monomer that results in a quasi-three dimensional network with poor π–π stacking. The broad peaks observed centred at $2\theta = 3.71°$, $5.01°$, and $6.9°$ for CTP-TAPB were roughly assigned to the [100], [200], and [220] facets, respectively. Similarly, for CTP-TCPB, the peaks observed at $2\theta = 3.65°$, $5.05°$, and $7.32°$ were assigned to the [100], [210], and [221] facets, respectively. The peak at the lower 2θ value corresponds to the [100] plane, whereas the broad peak in the range ~16–25° pertains to the [001] facets aroused from the π–π interaction between the successive layers. Moreover, the probable structures of the CTP-TAPB and CTP-TCPB were modelled using the Materials Studio software package in line with the previous report (Section S3,

ESI†).[13] Despite low crystallinity, a fair agreement between the simulated and experimental PXRD patterns suggests the proposed structures of the CTP-TAPB and CTP-TCPB frameworks. Subsequently, Pawley refinement was performed, which also manifested good agreement with AA-simulated packing patterns of CTP-TAPB and CTP-TCPB frameworks with minimal differences in the calculated and experimental patterns (Fig. S1 and S2, ESI†).

The chemical composition of the CTP-TAPB and CTP-TCPB frameworks was examined through Fourier-transform infrared (FT-IR) spectroscopy and ^{13}C cross-polarisation magic angle spinning nuclear magnetic resonance spectra (CP-MAS-NMR). FT-IR spectra of CTP-TAPB revealed a distinct band at 1625 cm^{-1}, confirming the C=N formation (Fig. 1b and Fig. S3, ESI†), while CTP-TCPB exhibited stretching bands at 1594 and 2252 cm^{-1} assigned to C=C and cyano (C≡N) functional groups, respectively, confirming the vinylene-linkage in the framework (Fig. 1b and Fig. S4, ESI†). Furthermore, as depicted in Fig. 1c, the resonance peak at 160 ppm in the ssNMR indicated the carbon peak characteristic of the C=N bond for CTP-TAPB, whereas for CTP-TCPB, the bands at 154 and 113 ppm were assigned to carbons of vinylene and the C≡N group, confirming the successful condensation of CTP-6-CHO and TCPB (Fig. S6 and S7, ESI†). To assess the porous nature of the frameworks, N$_2$ sorption studies were conducted at 77 K (Fig. S8, ESI†), revealing a Brunauer–Emmett–Teller (BET) surface area of approximately 30 m^2 g^{-1} for both frameworks. Thermogravimetric analysis (TGA) indicated good thermal stability up to 350 °C (Fig. S9, ESI†). Scanning and transmission electron microscopy images displayed a uniform spherical morphology for the CTP-TAPB and CTP-TCPB frameworks (Fig. 1d, Fig. S10 and S11, ESI†).

The photophysical properties of the frameworks were investigated by UV-Vis diffuse reflectance spectroscopy (DRS). Their DRS spectra exhibited absorption in the 300–400 nm range, with an absorption edge of 450 nm (Fig. 2a). The broad absorption feature of these materials is attributed to the presence of various crystalline domains and the high density of the defects in the solid-state. The photoluminescence (PL) spectra of the CTP-TAPB displayed a broad emission peak at 421 nm (λ_{ex} = 395 nm) (Fig. S13, ESI†), whereas CTP-TCPB exhibited the emission maximum at 420–520 nm (λ_{ex} = 380 nm), as shown in Fig. 2b, inset. We performed time-correlated single photon counting (TCSPC) experiments to measure the excited-state lifetime. The experimental decay curves were fitted with bi-component exponentials, and the average excited-state lifetime was estimated to be 0.15 and 0.17 ns for CTP-TAPB and CTP-TCPB, respectively (Fig. 2b and Fig. S14, ESI†). Furthermore, the direct band gap energies of both frameworks were extracted using the Tauc plot from their UV-Vis DRS absorption spectrum. The band gap values were calculated to be 2.94 and 2.88 eV for CTP-TAPB and CTP-TCPB, respectively (Fig. 2a). The HOMO and LUMO energy levels were determined using cyclic voltammetry (CV). The CV profiles of both frameworks were recorded in dry acetonitrile to measure the reduction potentials of these frameworks. The reduction potentials of −0.772 and −0.738 eV were observed for CTP-TAPB and CTP-TCPB, respectively (Fig. 2c and Section S13, ESI†). The positions of the HOMO
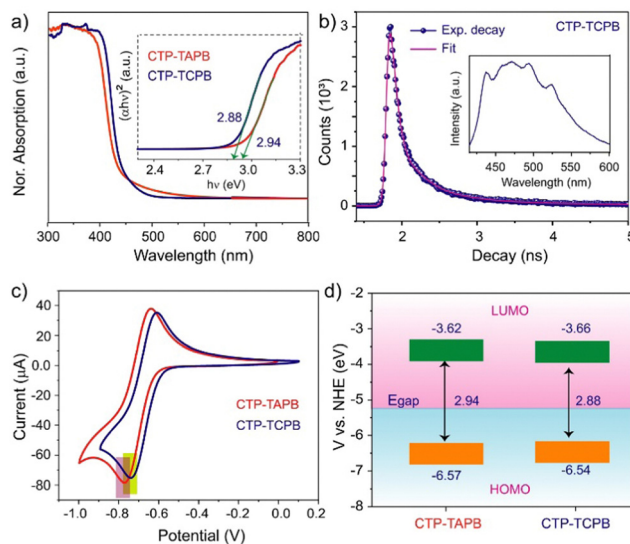

Fig. 2 (a) Electronic absorption spectra (inset: Tauc plots) of CTP-TAPB and CTP-TCPB, (b) excited state lifetime measurement of CTP-TCPB using the TCSPC method (inset: PL spectra), (c) CV studies (solvent: acetonitrile; scan rate 100 mV s^{-1}), (d) schematic energy level diagram of CTP-TAPB and CTP-TCPB frameworks obtained from optical band gap calculations and CV studies.

(E_{HOMO}) and LUMO (E_{LUMO}) were calculated from the reduction potentials and band gap energies (Fig. 2d and Table S1, ESI†). The HOMO and LUMO energy levels of CTP-TAPB are positioned at −6.57 and −3.62 eV, respectively. For CTP-TCPB, the E_{HOMO} and E_{LUMO} were found to be −6.54 and −3.66 eV, respectively.

Taking note of the successful integration of NLOphore and their intriguing optoelectronic properties, we investigated the NLO response of these frameworks employing the single-beam Z-scan technique, using an ultrashort pulsed fibre laser emitting 370 fs pulses at a repetition rate of 1 kHz. A detailed description of the experimental configuration and the measurement method is provided in Section S14, ESI.† The OA Z-scan transmittance is carried out with laser intensity varying in the range from 0.3 to 1.3 TW cm^{-2}, and the variation is shown in Fig. 3a (CTP-TAPB) and Fig. 3b (CTP-TCPB). The green spheres represent the transmission at lower pump intensity, whereas the curves with pink spheres show the NLO response at higher pump intensity. From the variation, it is apparent that both the frameworks undergo a shift from peak to valley in the OA transmittance (at z = 0) when the on-axis peak laser intensity changes in the aforementioned range (Fig. S16, ESI†). Alternatively, this presents a laser intensity-dependent switching from SA to RSA behaviour, which is marked by a change in the sign of β (Table 1). The experimentally measured OA transmittance traces are fitted to estimate the values of the NLA coefficient using a theoretical two-band model prescribed by Bahae et al.[14] The fitting recipe and a brief description of the fitting parameters are given in Section S14, ESI.† In the present work, we focus on the nonlinear optical spectroscopy of the organic frameworks with regard to possible applications in the field of devising optical limiters to be deployed in applications such as mode-locking of lasers, image contrast enhancement, optical
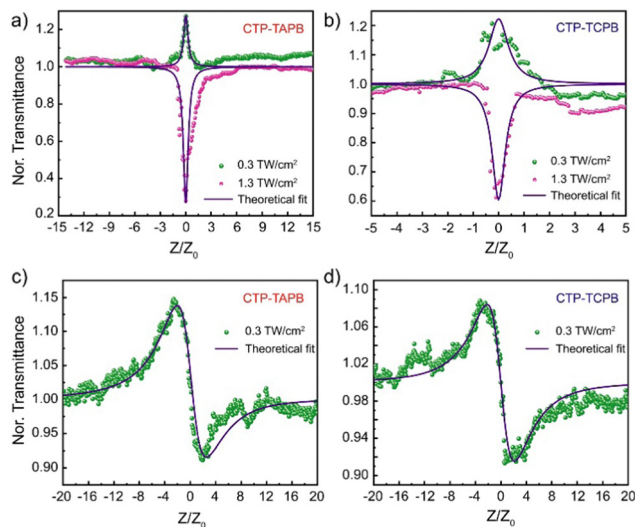
Fig. 3 Open aperture Z-scan measurements for (a) CTP-TAPB and (b) CTP-TCPB recorded with fs laser excitation at laser intensities of 0.3 TW cm^{-2} and 1.3 TW cm^{-2}, and closed aperture Z-scan measurements for (c) CTP-TAPB and (d) CTP-TCPB recorded with fs laser excitation at 0.3 TW cm^{-2} laser intensity.

Table 1 Nonlinear optical coefficients of CTP-TAPB and CTP-TCPB at the fixed excitation wavelength of 1030 nm

Sample	β (cm GW^{-1})		
	$I_0 = 0.3$ TW cm^{-2}	$I_0 = 0.8$ TW cm^{-2}	$I_0 = 1.3$ TW cm^{-2}
CTP-TAPB	−0.023	0.014	0.017
CTP-TCPB	−0.019	0.009	0.010

switching, *etc.* From Table 1, it is apparent that the change in the absolute value of β is very small as a function of on-axis peak laser intensity. However, as mentioned before, the sign of β changes at higher laser intensities. In order to appreciate this point, we note that out-of-plane covalent linking in both frameworks (CTP-TAPB and CTP-TCPB) may lead to a few vacant sites in the HOMO band. At low on-axis peak laser intensity, these contribute dominantly to the NLA process. Since these intervalence band absorptions (IVBA) are one-photon assisted transitions, the OA transmission exhibits a characteristic SA peak at beam focus ($z = 0$) when the on-axis peak laser intensity is low (0.3 TW cm^{-2}). On the other hand, the conventional three-photon assisted NLO transitions dominantly contribute to the NLA process at high on-axis peak laser intensity (Fig. 2d).

Consequently, we obtain a small positive β for both CTP-TAPB as well as CTP-TCPB when the laser intensity is high. It is quintessential to acknowledge the fact that the value of β estimated here is purely electronic owing to the low repetition rate of laser pulses (1 kHz) used in the OA Z-scan experiment. When identical measurements are carried out using nanosecond laser pulses, we obtain $\beta \sim 10^4$ cm GW^{-1}, which is essentially a consequence of accumulated thermal effect (ATE) (Table S2, ESI†). Moreover, the influence of linkage-type on NLO response has been investigated. The more efficient conjugation through the vinylene linkage was expected to afford a higher β value for

CTP-TCPB. However, under an fs laser, the β values for both frameworks were comparable. In contrast, the trend was more explicit under a ns laser and comparable to the reported values (Table S4, ESI†).

Additionally, closed-aperture (CA) Z-scan transmission has been measured to ascertain the nonlinear refractive index, which determines the optical switching characteristics of the frameworks. For CA Z-scan transmittance measurements, the repetition rate of the laser is fixed to 1 kHz and the pulse-width remains unchanged (370 fs). A low repetition rate ensures that the contribution of thermo-optic nonlinearities to the estimation of n_2 is negligible and therefore, the measured value of n_2 is predominantly electronic in origin. It is important to note that the underlying mechanism resulting in third-order optical nonlinearity exhibits a direct impact on the optical switching speed and from this perspective, the thermo-optic manifestations result in slower optical switching and usually, thermal nonlinearity induced n_2 has limited applications in optical communications systems. For CTP-TAPB and CTP-TCPB, the measured normalized transmittance in CA Z-scan is shown in Fig. 3c and d. The frameworks show a peak-to-valley variation, which results in a negative sign of n_2 signifying self-defocusing effect. The n_2 values are estimated to be -2.12×10^{-7} and -1.62×10^{-7} cm^2 GW^{-1} for CTP-TAPB and CTP-TCPB, respectively. The more efficient conjugation through the vinylene linkage in CTP-TCPB seems to have a negligible impact on n_2 as both the compounds exhibit comparable n_2 values. From the estimated values of n_2 for CTP-TAPB and CTP-TCPB, the complex third-order nonlinear susceptibility ($\chi^{(3)}$) is calculated to be -9.92×10^{-8} and -7.58×10^{-8} esu. The detailed steps followed for calculating $\chi^{(3)}$ are given in Section S14, ESI.† It is worthwhile to point out that the SA to RSA switching as a function of laser intensity (as observed in OA Z-scan transmission) provides a novel route to dynamically manoeuvre the optical limiting properties of all-dielectric organic frameworks for mode-locking relatively low-power lasing systems with high optical limiting efficiency.

In summary, imine (CTP-TAPB) and vinylene-linked (CTP-TCPB) 2D organic frameworks with a stereoscopic octupolar node have been synthesised and characterised. Leveraging the inherent NLO properties of the CTP core, the NLO property of both frameworks was evaluated. Interestingly, a switching of SA to RSA behaviour was observed for both frameworks. Furthermore, the effect of light intensity, ns and fs lasers, to alleviate the conventional thermal contribution of the ns laser towards the NLO properties of these materials is examined. In addition, the influence of linkage type (imine *vs.* vinylene) on NLO response has been discussed. Overall, this study reveals the vast opportunity of exploring NLO properties of organic frameworks by integrating the existing NLOphores to develop next-generation NLO switching materials.

Conflicts of interest

There are no conflicts to declare.

Notes and references

1 (a) C. S. Diercks and O. M. Yaghi, *Science*, 2017, **355**, eaal1585; (b) S. Kandambeth, K. Dey and R. Banerjee, *J. Am. Chem. Soc.*, 2018, **141**, 1807–1822; (c) K. T. Tan, S. Ghosh, Z. Wang, F. Wen, D. Rodríguez-San-Miguel, J. Feng, N. Huang, W. Wang, F. Zamora and X. Feng, *Nat. Rev. Methods Primers*, 2023, **3**, 1.

2 (a) S. Zhang, Q. Yang, C. Wang, X. Luo, J. Kim, Z. Wang and Y. Yamauchi, *Adv. Sci.*, 2018, **5**, 1801116; (b) Y. Tian and G. Zhu, *Chem. Rev.*, 2020, **120**, 8934–8986.

3 (a) R. Shi, X. Han, J. Xu and X. H. Bu, *Small*, 2021, **17**, e2006416; (b) J. Wolff and R. Wortmann, *Adv. Phys. Org. Chem.*, 1999, **32**, 121–217.

4 (a) M. Calvete, G. Y. Yang and M. Hanack, *Synth. Met.*, 2004, **141**, 231–243; (b) D. J. Li, Q. H. Li, Z. R. Wang, Z. Z. Ma, Z. G. Gu and J. Zhang, *J. Am. Chem. Soc.*, 2021, **143**, 17162–17169.

5 M. Li, C. Gong, J. Du, D. Ding, D. Du, D. Wang, J. Jiang, T. Li, C. Zheng, Y.-F. Yang, Y. She and J. Jia, *ACS Mater. Lett.*, 2023, **5**, 694–703.

6 (a) R. Medishetty, J. K. Zareba, D. Mayer, M. Samoc and R. A. Fischer, *Chem. Soc. Rev.*, 2017, **46**, 4976–5004; (b) Z. Z. Ma, Q. H. Li, Z. Wang, Z. G. Gu and J. Zhang, *Nat. Commun.*, 2022, **13**, 6347; (c) L. Zhang, H. Li, H. He, Y. Yang, Y. Cui and G. Qian, *Small*, 2021, **17**, e2006649; (d) H. S. Xu, Y. Luo, X. Li, P. Z. See, Z. Chen, T. Ma, L. Liang, K. Leng, I. Abdelwahab, L. Wang, R. Li, X. Shi, Y. Zhou, X. F. Lu, X. Zhao, C. Liu, J. Sun and K. P. Loh, *Nat. Commun.*, 2020, **11**, 1434.

7 (a) B. P. Biswal, S. Valligatla, M. Wang, T. Banerjee, N. A. Saad, B. M. K. Mariserla, N. Chandrasekhar, D. Becker, M. Addicoat and I. Senkovska, *Angew. Chem.*, 2019, **131**, 6970–6974; (b) M. Samal, S. Valligatla, N. A. Saad, M. V. Rao, D. N. Rao, R. Sahu and B. P. Biswal, *Chem. Commun.*, 2019, **55**, 11025–11028.

8 T. Wang, T. Sun, W. Tang, W. Huang, W. Zhang, L. Yan, J. Si and H. Ma, *New J. Chem.*, 2020, **44**, 15345–15349.

9 L. Zhang, Y. Zhou, M. Jia, Y. He, W. Hu, Q. Liu, J. Li, X. Xu, C. Wang, A. Carlsson, S. Lazar, A. Meingast, Y. Ma, J. Xu, W. Wen, Z. Liu, J. Cheng and H. Deng, *Matter*, 2020, **2**, 1049–1063.

10 (a) M. Yang, C. Mo, L. Fang, J. Li, Z. Yuan, Z. Chen, Q. Jiang, X. Chen and D. Yu, *Adv. Funct. Mater.*, 2020, **30**, 2000516; (b) J. Y. Zeng, X. S. Wang, B. R. Xie, M. J. Li and X. Z. Zhang, *Angew. Chem., Int. Ed.*, 2020, **59**, 10087–10094; (c) Z. Liu, B. Zhang, Y. Huang, Y. Song, N. Dong, J. Wang and Y. Chen, *iScience*, 2021, **24**, 102526; (d) H.-S. Xu, Y. Luo, X. Li, P. Z. See, Z. Chen, T. Ma, L. Liang, K. Leng, I. Abdelwahab and L. Wang, *Nat. Commun.*, 2020, **11**, 1–6; (e) J. Quertinmont, L. Maschio, A. Datta and B. Champagne, *J. Phys. Chem. C*, 2020, **124**, 24451–24459.

11 S. Nath, A. Puthukkudi, J. Mohapatra and B. P. Biswal, *Angew. Chem.*, 2023, **135**, e202218974.

12 (a) M. Basharat and D. Hadji, *J. Mater. Sci.*, 2022, **57**, 6971–6987; (b) P. C. Jha, A. Krishnan, P. K. Das and S. Ramasesha, *J. Chem. Phys.*, 2002, **117**, 2873–2881; (c) K. P. K. Naik, V. Sreeramulu, E. Ramya, K. Muralidharan and D. N. Rao, *Mater. Chem. Phys.*, 2016, **180**, 38–45.

13 (a) X. Guo, Y. Li, M. Zhang, K. Cao, Y. Tian, S. Qi, S. Li, K. Li, X. Yu and L. Ma, *Angew. Chem., Int. Ed.*, 2020, **59**, 22697–22705; (b) M. Zhang, Y. Li, C. Bai, X. Guo, J. Han, S. Hu, H. Jiang, W. Tan, S. Li and L. Ma, *ACS Appl. Mater. Interfaces*, 2018, **10**, 28936–28947.

14 M. Sheik-Bahae, A. A. Said, T.-H. Wei, D. J. Hagan and E. W. Van Stryland, *IEEE J. Quantum Electron.*, 1990, **26**, 760–769.